An Equilibrium Constitutive Model of Anisotropic Cartilage Damage to Elucidate Mechanisms of Damage Initiation and Progression

Michael E. Stender
Department of Mechanical Engineering,
University of Colorado,
Boulder, CO 80309

Richard A. Regueiro
Department of Civil, Environmental,
and Architectural Engineering,
University of Colorado,
Boulder, CO 80309

Stephen M. Klisch
Department of Mechanical Engineering,
California Polytechnic State University,
San Luis Obispo, CA 93407

Virginia L. Ferguson[1]
Department of Mechanical Engineering,
University of Colorado,
427 UCB, Boulder, CO 80309
e-mail: virginia.ferguson@colorado.edu

Traumatic injuries and gradual wear-and-tear of articular cartilage (AC) that can lead to osteoarthritis (OA) have been hypothesized to result from tissue damage to AC. In this study, a previous equilibrium constitutive model of AC was extended to a constitutive damage articular cartilage (CDAC) model. In particular, anisotropic collagen (COL) fibril damage and isotropic glycosaminoglycan (GAG) damage were considered in a 3D formulation. In the CDAC model, time-dependent effects, such as viscoelasticity and poroelasticity, were neglected, and thus all results represent the equilibrium response after all time-dependent effects have dissipated. The resulting CDAC model was implemented in two different finite-element models. The first simulated uniaxial tensile loading to failure, while the second simulated spherical indentation with a rigid indenter displaced into a bilayer AC sample. Uniaxial tension to failure simulations were performed for three COL fibril Lagrangian failure strain (i.e., the maximum elastic COL fibril strain) values of 15%, 30%, and 45%, while spherical indentation simulations were performed with a COL fibril Lagrangian failure strain of 15%. GAG damage parameters were held constant for all simulations. Our results indicated that the equilibrium post-yield tensile response of AC and the macroscopic tissue failure strain are highly dependent on COL fibril Lagrangian failure strain. The uniaxial tensile response consisted of an initial nonlinear ramp region due to the recruitment of intact fibrils followed by a rapid decrease in tissue stress at initial COL fibril failure, as a result of COL fibril damage which continued until ultimate tissue failure. In the spherical indentation simulation, damage to both the COL fibril and GAG constituents was located only in the superficial zone (SZ) and near the articular surface with tissue thickening following unloading. Spherical indentation simulation results are in agreement with published experimental observations. Our results indicate that the proposed CDAC model is capable of simulating both initial small magnitude damage as well as complete failure of AC tissue. The results of this study may help to elucidate the mechanisms of AC tissue damage, which initiate and propagate OA. [DOI: 10.1115/1.4030744]

Keywords: articular cartilage, damage modeling, finite-element analysis, anisotropy

Introduction

Injuries to AC can range from debilitating to undetectable, yet there is currently a limited understanding of the mechanisms that result in AC injuries and the long-term consequences of damage in vivo. The AC solid matrix (MAT) is composed primarily of type II COL fibrils and GAG molecules [1,2]. The COL fibrils contribute primarily to tissue integrity under uniaxial tensile loading [3] and Poisson's ratios of AC in unconfined compression [4–6]. GAG molecules impart an osmotic swelling pressure on the tissue that counteracts compressive loading [6–8] and imparts a prestress on COL fibrils [9,10]. Additionally, molecular level covalent and noncovalent interactions between GAG molecules and COL fibrils have an effect on the mechanical response of AC [3,10]. Additional constituents make up a small volume fraction of the cartilage solid MAT including cartilage cells, or chondrocytes, additional proteins, type IV COL fibrils, and other charged molecules and macromolecules [11,12]. Thus, the gross mechanical response of AC is derived from a superposition of individual constituent-specific responses and subtle interactive effects between constituents that depend on the applied loading condition.

Despite the demanding mechanical function of AC, it has poor intrinsic healing capability likely due to avascularity and low cell count [13]. AC is subject to varying degrees of traumatic injury and/or progressive degeneration that can result in OA as observed in animal and human studies [14–17]. AC injuries as a result of overloading have been observed to result in cell death and a decrease in the capability of AC to resist subsequent loading [18,19]. Due to the complexity of AC and the difficulty in experimentally assessing constituent-specific damage, relatively little is known about the consequences of AC injuries, particularly when injuries do not result in macroscopically visible AC damage.

Experimental studies of OA often aptly examine the differences between a healthy control group and an osteoarthritic group and thus, the resulting effects rather than the precise causes of OA are quantified experimentally. For example, variations in biochemical composition of AC with OA, such as increased water content and decreased GAG content, have been quantified [2,17,20]. In human patellar cartilage, early OA is characterized by decreased GAG

content and loss of COL fibril network organization, while late stage OA shows decreased COL content [21]. With OA, progressive fibrillation of COL fibrils, which results in decreased mechanical integrity of COL fibrils, a loss of COL fibril network organization, and AC thickening, has been observed to start at the surface and progress into deeper layers [17,22]. With OA and degeneration, AC has been observed to undergo both compositional and structural changes that lead to a decreased mechanical integrity and a progressive lessening of AC functionality.

The aim of this work is to expand on contemporary experimental studies using a computational model to better understand AC degradation and injury. Previous computational approaches have been implemented to study the characteristics of damage in COL fibril-reinforced soft tissues other than AC, which are not experimentally measurable or prohibitively difficult to measure experimentally. Recent stochastic finite strain models for fibril-reinforced soft tissues have been proposed without extensive validation [23–25]. Other studies have proposed constituent-based continuum damage models of aortic tissues including only damage to the fibrillar network [26] and damage to the nonfibrillar network and/or the tissue ground MAT [27,28] with varying degrees of validation. Also, while one study proposed a constitutive model specific to AC including damage to the ground MAT and the COL fibril constituents without experimental validation, this study was only 2D [29]. Therefore, the primary objective of this paper is to improve upon current models and expand our understanding of AC degradation by developing a 3D AC-specific CDAC model. This model is capable of highly anisotropic COL fibril damage (i.e., damage in any number of discrete COL fibril directions), and an isotropic GAG molecule damage formulation that captures GAG molecule leeching and cleaving as a result of deformation. To provide a validation of the results of the CDAC model, results from a spherical indentation simulation will be compared to experimental observations from similar loading scenarios of COL fibril damage and denaturation [30] and the locations of GAG molecule leeching and/or cleaving [31].

Materials and Methods

Preliminaries. The right Cauchy–Green deformation tensor, $\mathbf{C}$, is defined as

$$\mathbf{C} = \mathbf{F}^{\mathrm{T}}\mathbf{F} \qquad (1)$$

where $\mathbf{F}$ is the deformation gradient tensor. The Lagrangian strain tensor, $\mathbf{E}$, is defined as

$$\mathbf{E} = \frac{1}{2}(\mathbf{C} - \mathbf{I}) \qquad (2)$$

where $\mathbf{I}$ is the identity tensor. The directional Lagrangian strain implemented in this work to define COL fibril constituent material behavior is calculated as

$$E_N = \mathbf{N} \cdot (\mathbf{E}\mathbf{N}) \qquad (3)$$

where $\mathbf{N}$ is a unit normal direction vector in the reference configuration, and $(\cdot)$ is the dot product operator. Note that the vector and tensor operations required to calculate E_N return a scalar for the value of E_N in a direction, N. The second Piola-Kirchhoff stress tensor, $\mathbf{S}$, and the Cauchy stress tensor, $\mathbf{T}$, can be related via a push-forward operation as shown below

$$\mathbf{T} = \frac{1}{J}\mathbf{F}\mathbf{S}\mathbf{F}^{\mathrm{T}} \qquad (4)$$

where $J = \det \mathbf{F}$ is the determinant of the deformation gradient tensor. The second Piola-Kirchhoff stress tensor for a Green elastic material (eventually with damage) can be derived from the

Helmholtz free energy function per unit reference volume, ψ, using the following relationship:

$$\mathbf{S} = 2\frac{\partial \psi}{\partial \mathbf{C}} \qquad (5)$$

Similarly, the fourth-order material elasticity tensor in the reference configuration, $\mathbb{C}$, is derived as

$$\mathbb{C} = 2\frac{\partial \mathbf{S}}{\partial \mathbf{C}} \qquad (6)$$

For this study, a previous equilibrium constitutive model of AC [32] is extended to include damage to COL and GAG constituents. In the previous model, the mechanical response of AC is assumed to be a superposition of responses from an anisotropic COL fibril network, GAG molecules, and a ground substance MAT. Any viscoelastic effects are neglected. All constituents are hypothesized to be linked directly to the solid MAT. Thus, COL, GAG, and MAT constituents all experience the same deformation, $\mathbf{F}$, when loaded. The total solid MAT stress without damage is reported as a sum of COL, GAG, and MAT constituent stresses via a stress balance hypothesis. To enhance numerical convergence and to ensure material stability, ψ^{COL}, ψ^{GAG}, and ψ^{MAT} are all presented as convex functions of $\mathbf{F}$, $\mathbf{J}$, and $\mathbf{F}$, respectively [32,33]. As in Stender et al. [32], this CDAC model is developed for newborn (1–3 weeks old) bovine AC from the patellofemoral groove because of an existing comprehensive set of biomechanical, biochemical, and theoretical properties available for that specific tissue source [6,32]. Currently, there is not a similar comprehensive set of data available for other AC in mature or aging tissues. For a more complete summary of this previous model of AC, and a discussion of the results, refer to Stender et al. [32].

Anisotropic COL Fibril Damage Model. The COL fibril Helmholtz free energy function per unit reference volume, ψ^{COL}, is proposed to be a function of the true COL fibril Helmholtz free energy function per unit reference volume, $\check{\psi}^{\mathrm{COL}}$ and a dimensionless COL fibril damage parameter, d_N^{f}

$$\psi^{\mathrm{COL}} = \check{\psi}^{\mathrm{COL}}\big[1 - d_N^{\mathrm{f}}\big] \qquad (7)$$

where $0 \leq d_N^{\mathrm{f}} \leq 1$ in direction N. Note that here the damage parameter d_N^{f} represents the percent degradation of COL fibril material (damage is independent of loading) in direction N; e.g., $d_N^{\mathrm{f}} = 0$ implies no fibril damage while $d_N^{\mathrm{f}} = 1$ is 100% degraded fibril elastic strain energy. Note that Eq. (7) is a 1D relation in direction N that is later integrated over a unit sphere at each material point while allowing d_N^{f} to vary based on direction, thus allowing for 3D anisotropic COL fibril damage. The COL fibril damage parameter, d_N^{f}, is not to be confused with damage in ductile polycrystalline metals that are associated with void nucleation, growth, and coalescence, requiring the damage to be represented in the kinematics, as well as thermodynamics [34]. Thus, in this model there are no explicit damage-specific kinematic variables and consequently, no damage-specific conjugate stress terms. See the Appendix for discussion of the thermodynamics for this model. A constitutive assumption is made for a polyconvex form of the true COL fibril Helmholtz free energy function without damage per unit reference volume [32]

$$\check{\psi}^{\mathrm{COL}} = H(E_N)\frac{1}{2}E^{\mathrm{f}}(E_N)^2 \qquad (8)$$

where E^{f} is the COL fibril elastic modulus, and $H(E_N)$ is the Heaviside step function. H is a piecewise continuous function used in this work as defined below
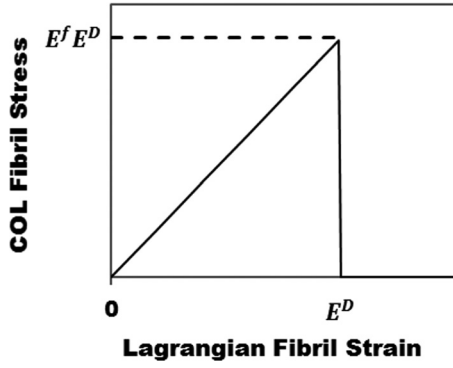
Fig. 1 The COL fibril constituent stress strain response with damage for a single COL fibril. All COL fibrils are hypothesized to initially respond with a linear elastic response and then fail completely if the COL fibril Lagrangian damage strain in direction N, E_N^D, value is exceeded. Thus, the maximum COL fibril yield stress in direction N is the product of the COL fibril modulus, E^f and the COL fibril Lagrangian failure strain, E_N^D in that direction.
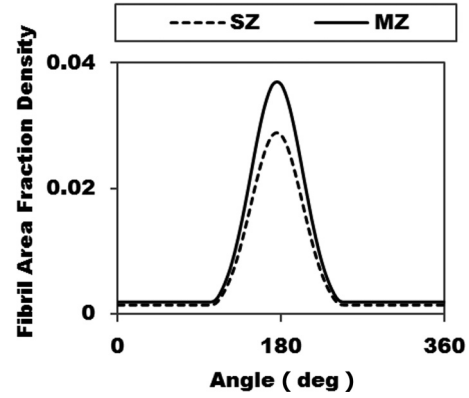

Fig. 2 Initial highly anisotropic COL fibril area density in the SZ and MZ of newborn bovine AC from the patellofemoral groove in a plane perpendicular to the articular surface. Initial COL fibril area fraction distributions are determined via quantitative polarized light microscopy measurements from Stender et al. [32] and adjusted for the biochemical COL fibril volume fraction from Williams et al. [6]. Note that angle = 90 deg corresponds to the direction perpendicular to the articular surface.

$$H(f(x)) = \begin{cases} 1, & f(x) > 0 \\ 0, & f(x) \le 0 \end{cases} \tag{9}$$

(i.e., COL fibrils are only active in tension). Note that the assumed form of $\check{\psi}^{COL}$ results in a linear stress–strain response for COL fibrils, which has been shown to be appropriate for immature bovine tissue [32]. However, this assumption may not be appropriate for more mature tissues, or other species and/or locations (see "Discussion section" for additional details).

COL fibrils are assumed to exhibit an elastic brittle damage response wherein COL fibrils exhibit a linear elastic response until Lagrangian fibril strain exceeds the Lagrangian failure strain of a COL fibril, E_N^D (i.e., the maximum elastic strain of a COL fibril) as shown in Fig. 1.

The COL fibril damage parameter, d_N^f is introduced as shown below

$$d_N^f = \begin{cases} 1, E_N > E_N^D \\ 0, E_N \le E_N^D \end{cases} \tag{10}$$

where d_N^f for undamaged, intact fibrils (i.e., COL fibril strain, $E_N \le E_N^D$), and $d_N^f = 1$ for damaged fibrils (i.e., COL fibril strain, $E_N \le E_N^D$). The COL fibril damage parameter, d_N^f, is defined and exists for any n number of discrete pyramidal volume elements at a material point each with a unique direction, N. Initially, all fibrils are assumed to be undamaged. The loading history is tracked such that once damaged, COL fibril healing and/or repair is disallowed. For a complete description of the COL fibril damage evolution formulation used in this model including a discussion of the capability to implement alternative forms of d_N^f and the tracking of COL fibril damage history, refer to the Appendix.

Previous soft tissue models have used continuous (i.e., nondiscrete) continuum fibril models to study soft fibrous tissues [35–38]. Specifically, the continuous fibril model of the anisotropic COL fibril network in AC used here was developed by Shirazi et al. [39] and is implemented by discretizing a unit sphere at each material point into N number of pyramidal volume elements. Each pyramidal volume element is then assigned a variable volume fraction of COL fibrils, φ_N^f, in direction N capturing the directional dependence of the COL network at the material point level. Note that when φ_N^f is integrated over the unit sphere, the result is equivalent to the experimentally measured COL fibril tissue volume fraction, φ^f which is combined with COL fibril spatial distribution imaging studies to define a realistic and anisotropic

COL fibril constituent. For a complete summary of the determination of and implementation of the anisotropic COL fibril distributions used here, refer to Stender et al. [32]. In summary, based on experimental results that Poisson's ratios and tensile modulus do not depend on direction in the plane parallel to the articular surface for newborn bovine AC from the patellofemoral groove, [6,40] COL fibril distributions were assumed to not vary in the plane parallel to the articular surface. Planar quantitative polarized light microscopy images were used to estimate COL fibril distribution in a plane perpendicular to the articular surface. COL fibril area fraction distributions in the plane perpendicular to the articular surface were determined from quantitative polarized light microscopy measurements [32] and adjusted based on experimental COL fibril tissue volume fraction [6]. A background isotropy and a normalized Gaussian distribution were assumed with the result as shown in Fig. 2.

Using Eqs. (7), (8), and (10), the COL constituent free energy function per unit reference volume, ψ^{COL}, is extended from Stender et al. [32] to include COL constituent damage as

$$\psi^{COL} = \frac{1}{4\pi} \int_{\phi=0}^{2\pi} \int_{\theta=0}^{\pi} H(E_N) \varphi_N^f \frac{1}{2} E^f (E_N)^2 \left[1 - d_N^f \right] \sin\theta d\theta d\phi \tag{11}$$

where θ and ϕ are angles within a spherical coordinate system to determine the unit direction vector $\mathbf{N} = \cos(\theta)\sin(\phi)\hat{\boldsymbol{\imath}} + \sin(\phi)\hat{\boldsymbol{J}} + \cos(\phi)\hat{\boldsymbol{k}}$, with associated Lagrangian strain E_N in Eq. (3). With the assumptions of a unit sphere at each material point and a local spherical coordinate system, $V = 4\pi/3$ and $dV = (1/3)\sin\theta d\theta d\phi$. Note that this formulation is developed from Shirazi et al. [39] and involves an integration within the unit sphere rather than on the unit sphere as other studies have proposed [36,37]. For a discussion of the equivalence of the integration approach presented here, and other models where integration is performed on the unit sphere refer to Stender et al. [32]. Using the relationship in Eq. (5), the COL fibril second Piola-Kirchhoff stress tensor, $\mathbf{S}^{COL}$, is obtained as

$$\mathbf{S}^{COL} = \frac{1}{4\pi} \int_{\phi=0}^{2\pi} \int_{\theta=0}^{\pi} H(E_N) \varphi_N^f E^f E_N \left[1 - d_N^f \right] [\mathbf{N} \otimes \mathbf{N}] \sin\theta d\theta d\phi \tag{12}$$

where $\otimes$ denotes the dyadic product. The COL fibril constituent material elasticity tensor can be similarly obtained using Eq. (6) and represented in indicial notation as
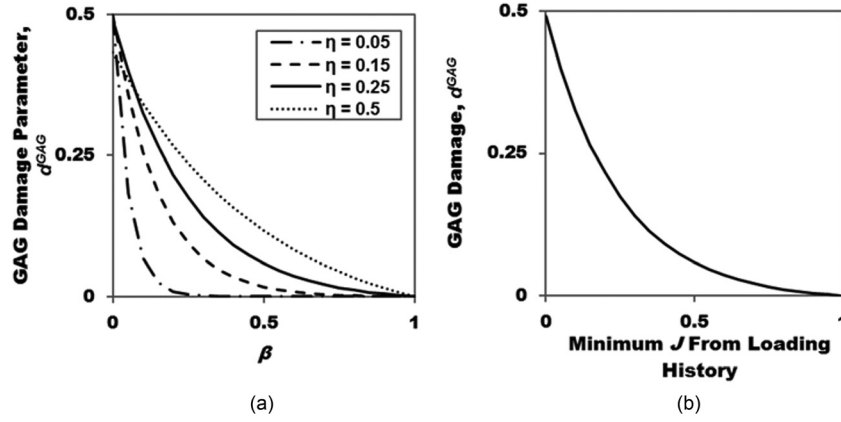
Fig. 3 GAG damage parameter, d^{GAG}, plots showing (*a*) d^{GAG} as a function of GAG damage ISV, β, for several values of the GAG damage scaling variable, η, with $d^{GAG}_{max} = 0.5$. (*b*) GAG damage, d^{GAG}, plotted for values of $d^{GAG}_{max} = 0.5$ and $\eta = 0.25$ as used in this study as a function of the minimum $J = \det F$ value in the material loading history.

$$\mathbb{C}^{COL}_{ABCD} = \frac{1}{4\pi} \int_{\phi=0}^{2\pi} \int_{\theta=0}^{\pi} H(E_N) \varphi_N^f E^f \left[1 - d_N^f\right] N_A N_B N_C N_D \sin\theta d\theta d\phi$$

(13)

For a more complete derivation of $\mathbf{S}^{COL}$ and $\mathbb{C}^{COL}_{ABCD}$ refer to the Appendix. The extent of COL fibril damage, D_{col} (%) is calculated in the user-defined material subroutine (UMAT) for each material point as the ratio between number of pyramidal elements at each material COL fibril damage has occurred at any point in the loading history, N_f^D, and the total number of pyramid elements, N_{total}, as shown in the following relationship:

$$D_{COL}(\%) = \frac{N_f^D}{N_{total}} * 100$$

(14)

Note that D_{COL} does not specifically quantify the anisotropic nature of COL fibril damage, but is implemented as a parameter to quickly quantify the extent of COL fibril damage at a material point.

GAG Damage Model. In addition to anisotropic COL fibril damage, an isotropic damage model of the GAG constituent of AC is also proposed. Here, GAG damage is assumed to be isotropic at each material point and to only occur during decreases in tissue volume. Thus, it is assumed that decreases in tissue volume result in leeching and/or cleaving of GAG molecules resulting in an effective decrease in GAG molecular density which is considered to be analogous to GAG damage. For a more complete examination of GAG damage assumptions, refer to "Discussion section." The total GAG Helmholtz free energy function per unit reference volume, ψ^{GAG}, is defined as

$$\psi^{GAG} = \breve{\psi}^{GAG}[1 - d^{GAG}]$$

(15)

where $\breve{\psi}^{GAG}$ is the undamaged GAG constituent free energy function per unit reference volume, and d^{GAG} is a GAG-specific damage parameter. The polyconvex GAG constituent Helmholtz free energy function per unit reference volume without damage was derived based on a curve fit to numerical results [32] from the Poisson–Boltzmann continuum electromechanical model as applied to GAG molecules [41] and is presented as

$$\psi^{GAG} = -\alpha_1 \frac{((\rho_0^{GAG})^{\alpha_2} \mathbf{J}^{(1-\alpha_2)})}{(1-\alpha_2))}$$

(16)

where α_1, $(MPa * ml^{2.5}/mg^{2.5})$ and α_2(unitless) are GAG material constants, and ρ_0^{GAG}, (mg/ml) is the mass density of GAG molecules in the tissue in the reference configuration. The evolution of GAG damage parameter, d^{GAG}, is proposed as an example function based on hypothesized GAG damage behavior as a novel function of the dimensionless GAG damage-related internal state variable (ISV) β which is equal to the minimum J value in the material loading history, the dimensionless GAG damage scaling parameter η, and the maximum attainable GAG damage scaling parameter d^{GAG}_{max}, with $0 \leq d^{GAG}_{max} \leq 1$

$$d^{GAG} = d^{GAG}_{max} \left[e^{\left(\frac{-\beta}{\eta}\right)} - e^{\left(\frac{-1}{\eta}\right)}\right]$$

(17)

Note that the precise form of d^{GAG} is unknown, and alternative forms of Eq. (17) may be easily integrated into this model. Several plots of d^{GAG} with $d^{GAG}_{max} = 0.5$ are shown in Fig. 3(*a*). In all simulations, $\eta = 0.25$ and $d^{GAG}_{max} = 0.5$ are used to demonstrate appreciable GAG damage with volumetric decreases for the simulations in this study as shown in Fig. 3(*b*).

The GAG-specific damage function, f^{GAG}, that tracks the occurrence and accumulation of GAG constituent damage is defined as

$$f^{GAG} = (\beta - J)(H(\beta - J))$$

(18)

where $J = \det \mathbf{F}$, the determinant of the deformation gradient tensor, $\mathbf{F}$. If $J \geq \beta$ (volumetric expansion greater than ISV β), then $f^{GAG} = 0$ and no damage has occurred. If $J < \beta$ (volumetric contraction) then $f^{GAG} = (\beta - J)$ and additional GAG damage has occurred. For this study, GAG molecules are assumed to be initially undamaged and thus, the initial value of the ISV β is set to $\beta_0 = 1$ such that $d_0^{GAG} = 0$. Similarly to the COL fibril damage model, a relationship is assumed in order to solve for the incremental change of the GAG damage state variable, $\delta\beta$ as shown below

$$\delta\beta = -f^{GAG}$$

(19)

when $f^{GAG} = (\beta - J)$, Eq. (19) gives $\delta\beta = -(\beta - J)$ and the damage-like ISV β evolves (decreases). For the case of $f^{GAG} = 0$ Eq. (19) gives $\delta\beta = 0$ and thus, additional GAG damage has not occurred and there is no evolution of the damage-like ISV, β. Note that for the GAG constituent, healing and/or repair of GAG molecules is effectively disallowed as the value of β can never increase.

Table 1 Experimental biochemical properties for bovine AC in the superficial and MZs established in a previous study [6] and used herein

	Water content (% tissue mass)	GAG molecule density, ρ_0^{GAG} (mg/ml)	COL fibril volume fraction, φ^f (% tissue volume)
SZ	89.3 ± 2.6	32.8 ± 7.5	3.9 ± 1.0
MZ	86.6 ± 2.8	47.6 ± 12.1	5.0 ± 1.4

Table 2 Predicted AC constituent GAG, ground substance MAT, and COL fibril mechanical properties for the SZ and MZ not related to damage used in this study established previously by Stender et al. [32]. Note that GAG constants are identical in the SZ and the MZ.

GAG constants	$\alpha_1 \left(MPa * ml^{2.5}/mg^{2.5} \right)$	2.87
	α_2	2.5
MAT constants	μ (SZ, MPa)	0.001
	μ (MZ, MPa)	0.001
COL Constants	E^f (SZ, MPa)	175
	E^f (MZ, MPa)	422

The complete GAG constituent energy density function per unit reference volume, ψ^{GAG}, is obtained by substituting Eqs. (16) and (17) into Eq. (15) as

$$\psi^{GAG} = -\alpha_1 \frac{(\rho_0^{GAG})^{\alpha_2} J^{(1-\alpha_2)}}{(1-\alpha_2)} \left\{ 1 - d_{max}^{GAG} \left[e^{\left(\frac{-\beta}{\eta}\right)} - e^{\left(\frac{-1}{\eta}\right)} \right] \right\} \quad (20)$$

The damage-enabled GAG constituent second Piola-Kirchhoff stress can then be derived using Eq. (5) as

$$\mathbf{S}^{GAG} = J\mathbf{F}^{-1} \left(-\alpha_1 \left(\rho_0^{GAG}/J \right)^{\alpha_2} \left\{ 1 - d_{max}^{GAG} \left[e^{\left(\frac{-\beta}{\eta}\right)} - e^{\left(\frac{-1}{\eta}\right)} \right] \right\} \right) \mathbf{F}^{-T} \quad (21)$$

Note that GAG stress is directly dependent on GAG molecule concentration via the ρ_0^{GAG}/J term in Eq. (21), which is equal to GAG molecule concentration in the current configuration. The damage-enabled GAG material stiffness tensor is derived using Eq. (6) with the result shown below in indicial notation

$$\mathbb{C}_{ABCD}^{GAG} - \left\{ \alpha_1 (\rho_0^{GAG})^{\alpha_2} (C_{AC}C_{BD} + C_{AD}C_{BC}) \right. $$
$$\left. + \alpha_1 \alpha_2 (\rho_0^{GAG})^{\alpha_2} C_{DC}^{-1} C_{AB}^{-1} \right\} \left\{ (\det C)^{-\frac{\alpha_2}{2}} \right\} \left\{ 1 - d_{max}^{GAG} \left[e^{\left(\frac{-\beta}{\eta}\right)} - e^{\left(\frac{-1}{\eta}\right)} \right] \right\} \quad (22)$$

The extent of GAG damage is easily quantified by the value of the GAG damage parameter, d^{GAG}, which corresponds to the percent decrease in effective GAG molecule concentration.

MAT Model. The MAT free energy function per unit reference volume was assumed to be a compressible Neo-Hookean strain energy function as proposed in Stender et al. [32] as

$$\psi^{MAT} = \frac{1}{2}\mu[(tr(\mathbf{C}) - 3) - \ln(\det(\mathbf{C}))] \quad (23)$$

where μ(MPa) is a MAT constituent shear modulus parameter. Because the results of Stender et al. [32] indicated that the MAT constituent did not have a significant contribution to the mechanical response of AC tissue from the newborn bovine patellofemoral groove (i.e., $\mu \approx 0$), damage to the MAT constituent is not considered in this work. Using Eqs. (5) and (23), the MAT constituent second Piola-Kirchhoff stress is derived as

$$\mathbf{S}^{MAT} = \mu(\mathbf{I} - \mathbf{C}^{-1}) \quad (24)$$

and the MAT constituent elasticity tensor in the reference configuration is derived in indicial notation using Eq. (6) as

$$\mathbb{C}_{ABCD}^{MAT} = \mu(C_{AC}^{-1}C_{BD}^{-1} + C_{AD}^{-1}C_{BC}^{-1}) \quad (25)$$

Previous Experimental and Computational Data. Experimental biomechanical and biochemical data from previous studies were used in the implementation of the CDAC model. The AC tissue was taken from the native newborn bovine patellofemoral groove from either the SZ or the middle zone (MZ).

A summary of tissue biochemical parameters used as model inputs can be found in Table 1. Biochemical values for GAG content and COL fibril volume fraction were available from Williams et al. [6]. Initial anisotropic COL fibril spatial distributions were determined *via* quantitative polarized light microscopy measurements [32] adjusted for the biochemical COL fibril volume fraction from Williams et al. [6].

AC material constants not associated with COL fibril or GAG molecule damage parameters are used in this work as presented in Stender et al. [32] for the same tissue source and are listed in Table 2. GAG material constants α_1 and α_2 were obtained from a fit to a Poisson–Boltzmann continuum electromechanical model [41] and are used as constant values. However, because the reference GAG densities differ between the SZ and MZ, the resulting GAG stress–strain equations are regionally dependent. Note that these AC model parameters are derived from fits to tensile and compressive biomechanical test data and represent the best possible fit to the initially undamaged response of AC from the newborn bovine patellofemoral groove.

Finite-Element Implementation and Simulations. Damage-enabled GAG and COL constitutive models were implemented in ABAQUS v6.13 using the UMAT capability. The COL fibril, GAG molecule, and MAT constituent material stiffness tensors (Eqs. (13), (22), and (25), respectively) were transformed to the Jacobian, or the tangent stiffness MAT, $\mathbb{C}_{ijkl}^{jac}$, where *jac* stands for Jacobian, as required by ABAQUS (for full derivation see Stender et al. [32]) using the following relationship shown in indicial notation:

$$\mathbb{C}_{ijkl}^{jac} = \frac{1}{J}\left\{ \frac{1}{2}(\delta_{il}\tau_{jk} + \delta_{jk}\tau_{il} + \delta_{ik}\tau_{jl} + \delta_{jl}\tau_{ik} + \mathbb{C}_{ABCD}F_{iA}F_{jB}F_{kC}F_{lD}) \right\} \quad (26)$$

where is τ_{ij} the Kirchhoff stress, and δ_{ij} is the Kronecker delta. To enforce the loading history dependence of the CDAC model, additional state variables were required. The COL fibril ISV as discussed in the Appendix is defined as γ_N^f. GAG and COL fibril constituent ISV damage equations were coded directly in the UMAT. If the state variable values evolved as determined by the constituent state variable relationships, the evolution of state variables was calculated as shown below for COL and GAG damage-like ISVs, respectively, as

$$\gamma_{N(n+1)}^f = \gamma_{N(n)}^f + \delta\gamma_N^f, \quad \beta_{n+1} = \beta_n + \delta\beta \quad (27)$$

where $\gamma_{N(n+1)}^f$ and β_{n+1} are the state variable values at the end of the current solution step, and $\gamma_{N(n)}^f$ and β_n are the state variable values from the previous solution step. The evolution of COL and GAG damage-like ISVs, $\delta\gamma_N^f$ and $\delta\beta$, is determined from the evolution of the state variables in the current step defined in Eqs. (A3) and (19) for COL and GAG constituents, respectively.

To study the results of this proposed constitutive damage model of AC, two different finite-element models were developed in ABAQUS 6.13. First, a uniaxial stress in tension model consisting of
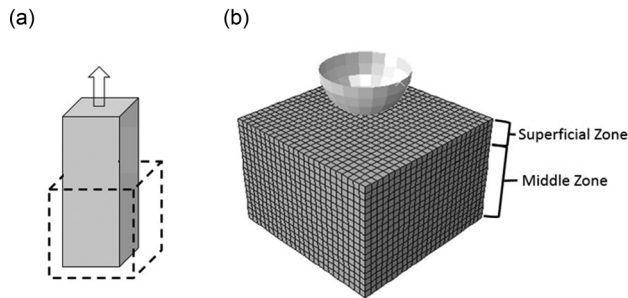
Fig. 4 Finite-element models showing (a) uniaxial stress in tension finite-element model with dashed lines denoting the initial configuration. (b) Spherical indentation model with superficial and MZs of AC. For spherical indentation simulations, the spherical indenter was modeled as an analytical rigid surface while the cartilage block was modeled using 10,625, eight-node linear hexahedral C3D8 elements with displacements at the bottom surface constrained in all directions. The adjacent SZ and MZ of regions were constrained at the shared surface using a tied contact formulation.

a single linear hexahedral element (C3D8) with full integration was developed and used to model AC damage and failure in uniaxial stress in tension loading (Fig. 4(a)). Due to the initial stress of the GAG constituent, to reach an initial equilibrium configuration, all simulations initially solve for an equilibrium stress state in an unloaded solution step [32]. For uniaxial tension simulations, tissue failure was defined to occur when the uniaxial tensile stress decreased to $\leq 1\%$ of the maximum uniaxial tensile stress. Second, a 3D finite-element model of a spherical indentation test was constructed consisting of 10,625 linear hexahedral elements with full integration and a rigid half sphere indenter. The cartilage sample was assumed to have dimensions of $1.0\,\text{mm} \times 1.0\,\text{mm} \times 0.7\,\text{mm}$ with a SZ 0.2 mm thick adjacent to the indenter and a 0.5 mm thick MZ directly beneath the SZ (Fig. 4(b)). The adjacent SZ and MZ zones were connected via a tied contact constraint. The rigid spherical indenter had a radius of 0.25 mm. Similarly to the uniaxial stress in tension model, all indentation simulations initially solve for an equilibrium stress state in an unloaded solution step. Following equilibrium, the indenter was displaced into the tissue to a depth of 0.06 mm for two cycles using a surface-to-surface contact algorithm for finite sliding and assuming frictionless contact. For uniaxial stress in tension simulations, the COL fibril damage strain parameter, E_N^D, was simulated as 0.15, 0.30, and 0.45 while spherical indentation simulations used $E_N^D = 0.15$. GAG damage parameters were assumed as $d_{\max}^{\text{GAG}} = 0.5$ and $\eta = 0.25$ for all simulations. Initial ISVs for COL and GAG constituents were set as $\gamma_{N(0)}^{\text{f}} = 0$ and $\beta_0 = 1$, respectively, for all simulations. To improve the solution computation time, the number of COL constituent pyramidal elements at material points was decreased to 200 for the spherical indentation simulation compared to 3200 for uniaxial stress in tension simulations. Mesh convergence studies for uniaxial stress in tension and spherical indentation simulations were performed. Because of the equilibrium nature of this model, time-dependent effects, such as viscoelasticity and poroelasticity, were neglected, and thus all results represent the equilibrium response after all time-dependent effects have dissipated.

Results

AC Damage Model. An initial unloaded equilibrium step resulted in slight volumetric swelling as a consequence of the intrinsic swelling of GAG molecules. No GAG or COL fibril constituent damage was incurred during the initial equilibrium swelling. During tensile loading, predicted macroscopic tissue failure strains from the CDAC model were highly dependent on the COL fibril failure strain, E_N^D (Fig. 5). For all uniaxial tensile
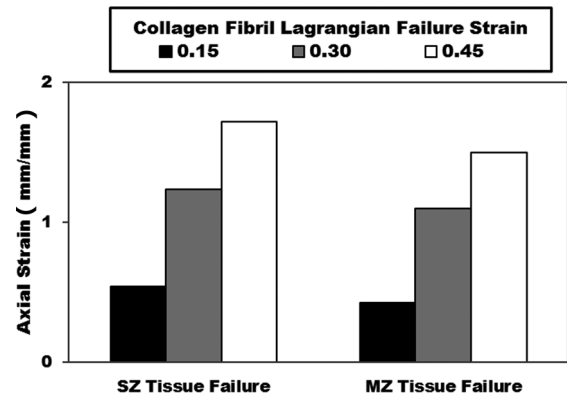

Fig. 5 Predicted equilibrium values of AC ultimate tensile failure strain for COL fibril Lagrangian failure strain values $E_N^D = 0.15, 0.30, 0.45$ in the SZ and MZ of bovine AC. Macroscopic AC tissue failure strain values were determined as when the tissue axial tensile stress reached 1% of the max stress.

failure simulations, COL fibril damage was the primary cause of macroscopic tissue failure.

In general, the tensile stress–strain response up to ultimate tissue failure behavior was found to be similar in the SZ and the MZ. Due to the strain-based COL fibril failure criterion, higher ultimate tensile stresses were observed in the MZ which has a higher theoretical COL fibril modulus compared with the SZ (Fig. 6).

Values of the COL spatial damage parameter, D_{col}, indicate severe extents of COL fibril damage at macroscopic tissue failure. In the SZ, D_{col} was calculated at tissue failure as 40.0%, 47.1%, and 49.1% for COL fibril damage strain values of 0.15, 0.30, and 0.45, respectively. In the MZ, D_{col} was calculated at tissue failure as 34.4%, 45.5%, and 46.8% for COL fibril damage strain values of 0.15, 0.30, and 0.45, respectively (Fig. 7). Additional dependence was found on E_N^D with higher values of E_N^D leading to higher predicted ultimate stress values and macroscopic tissue failure strain in all cases.

Due to COL damage with uniaxial tensile loading, the effective tissue COL fibril area fraction distributions of intact fibrils were found to vary greatly before and after uniaxial tension loading to failure. In tensile failure simulations, COL fibril damage is primarily aligned in the direction of tensile loading (Fig. 8). At macroscopic tissue failure, not all COL fibrils were damaged, with some fibrils (less than 12% by volume fraction in all simulations) oriented perpendicular to the direction of loading left intact.

In all uniaxial tension simulations, small amounts of GAG damage (between 0.4% and 6.6%) occurred. In all cases, GAG damage occurred just after the onset of tensile loading due to a slight
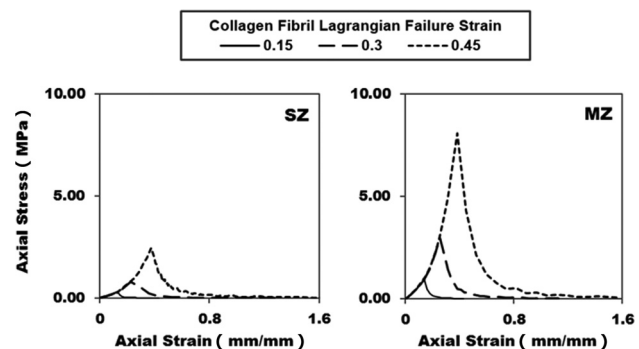

Fig. 6 Predicted equilibrium uniaxial tension axial stress strain response in the SZ and MZ for COL fibril Lagrangian failure strain values of $E_N^D = 0.15, 0.30, 0.45$. Vertical axis range is uniform for ease of comparison.

Fig. 7 Predicted equilibrium COL fibril damage, D_{col} (%), in the SZ and MZ for COL fibril Lagrangian failure strain values of $E_N^D = 0.15, 0.30, 0.45$. Vertical axis range is uniform for ease of comparison.
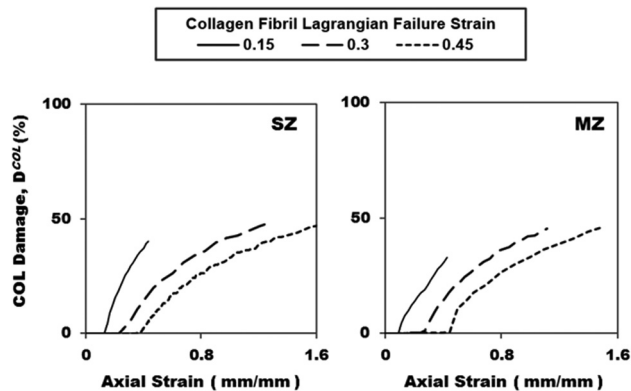
volumetric decrease in the tissue. During uniaxial tensile loading, all GAG damage values were small and did not propagate with additional uniaxial tensile loading.

Spherical Indentation Simulation. Initial unloaded equilibrium swelling did not result in GAG or COL damage in bilayered spherical indentation simulations. Locations of both GAG (Fig. 9(a)) and COL (Fig. 9(b)) damage at peak loading coincided with high-strain regions that were concentrated directly beneath the indenter tip.

All damage to both COL and GAG constituents was found only in the SZ. During indentation, GAG damage occurred at initial contact, while COL damage required higher indentation depths to occur. With increasing indenter tip displacement into the tissue, GAG damage progressed further from the articular surface and increased in magnitude. COL fibril constituent damage was located almost entirely at, or very near, the articular surface and increased in magnitude with increasing indenter tip displacement into the tissue. Compared with GAG damage, COL fibril damage did not progress as far from the articular surface. The maximum principal logarithmic (LE) strain contour plot (Fig. 9(c)) shows that strain was primarily concentrated in the SZ while the MZ experienced relatively small deformations. Similarly, the maximum principal stress contour plot (Fig. 9(d)) demonstrates that the

maximum tensile stresses are concentrated in the SZ near the interaction with the indenter tip, and maximum compressive stresses are again found in the SZ beneath the indenter tip. Increasing indentation depth resulted in a progressive damage response for both COL and GAG constituents (Fig. 10).

Following damage-inducing loading, a small amount of AC thickening was observed at the articular surface (Fig. 11). Additionally, a small amount of hysteresis due to both GAG and COL damage between the initial and second indentation cycles was observed in the reaction force on the indenter tip with reaction force decreasing during the second loading cycle. Indentation force values at maximum indentation depth were similar with a difference of 0.5% between cycles (Fig. 11). A mesh convergence study for the spherical indentation simulation indicated that the finite-element mesh as presented was sufficiently refined.

Discussion

Reduction in the mechanical integrity of AC due to damage, degradation, and disease has been well-documented experimentally [17,19,42–44]. Recently, computational modeling has emerged as a means of studying the mechanical response of AC tissue under various conditions [38,45–47] including the study of AC degeneration and damage [29,48]. Therefore, in this study, a previously developed equilibrium constitutive model of AC [32] was updated to include damage formulations for both COL and GAG constituents creating a highly anisotropic 3D CDAC model. In the CDAC model, healing and/or repair of either GAG or COL constituents is disallowed. Previously published experimental biochemical [6], biomechanical [6], and computational [32] parameters for newborn bovine AC from the patellofemoral groove were integrated to create a high-fidelity anisotropic 3D constitutive model that could be implemented in a finite-element analysis software package. In this study, newborn bovine tissue from the patellofemoral groove is studied because a more comprehensive set of experimental data was currently not available for another tissue source. The MAT constituent of AC is included herein to improve numerical model convergence properties and to facilitate expansion of this model to additional tissue sources that may have more influential MAT constituent responses. For example, GAG molecule concentration and COL fibril volume fraction vary between immature and adult bovine [40] tissue which may result in a higher MAT shear modulus, μ, for adult AC compared to immature AC tissue. To determine the effects of ultimate COL fibril strain, E_N^D, a single element finite-element model of a uniaxial
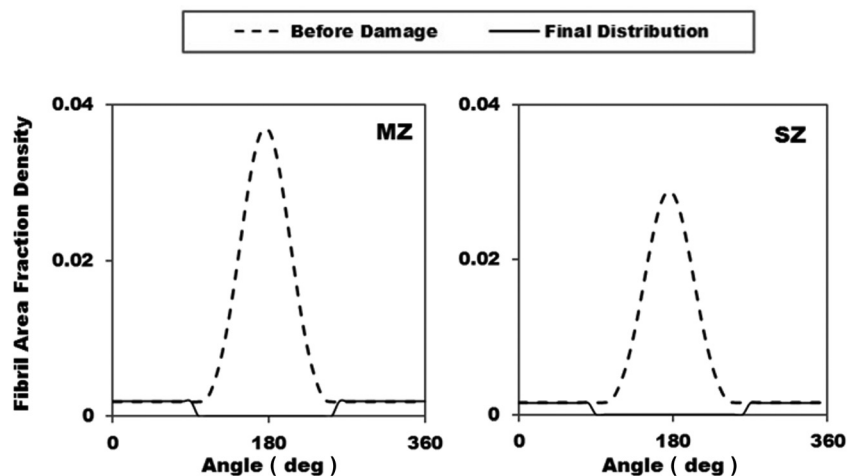

Fig. 8 Comparisons of COL fibril area fraction distribution in the MZ and SZ in undamaged tissue, and at the point of ultimate macroscopic tensile failure for a Lagrangian failure strain of $E_N^D = 0.30$. Note that uniaxial tensile load was aligned parallel to the articular surface in the 180 deg direction. Vertical axis range is the same for ease of comparison.
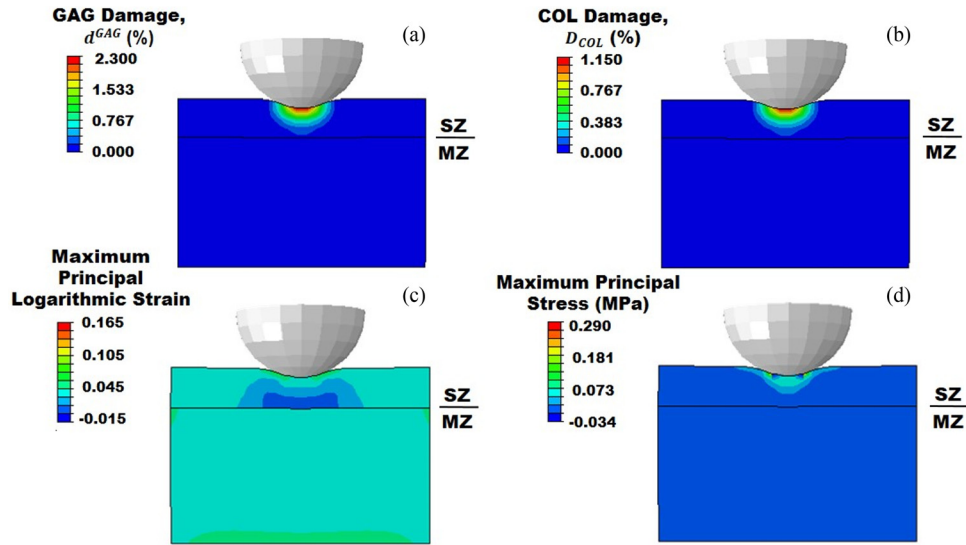
Fig. 9 Contour plots of finite-element analysis results for (*a*) GAG damage parameter, d^{GAG}, (*b*) COL fibril damage parameter, D_{col}, (*c*) maximum principal LE strain, and (*d*) maximum principal Cauchy stress (MPa) in a bilayered AC model with discrete SZ and MZ. A rigid spherical indenter was displaced into the articular surface while displacements in all directions at the bottom of the MZ were held fixed. Damage parameters of $E_N^D = 0.15$, $d_{max}^{GAG} = 0.5$, and $\eta = 0.25$ were used. Mesh lines removed for clarity.

tensile test was created and run to macroscopic tissue failure with a range of E_N^D values. In addition, a spherical indentation of AC with discrete SZ and MZ layers was simulated using finite-element analysis. All simulations required an initial unloaded equilibrium step where GAG swelling pressure is balanced by COL and MAT constituents resulting in a small volumetric expansion. With this GAG molecule formulation it is not possible to explicitly reach an unloaded GAG reference configuration. If future experiments show that it is absolute strain of the GAG molecules, rather than the strain relative to the GAG unloading state (i.e., equilibrium) that is influential on GAG damage, a different GAG formulation may be more appropriate. Neither GAG nor COL fibril damage was calculated in equilibrium solution steps because there was no volumetric compression to cause GAG damage, and the expansion strains were sufficiently small as to not damage to

COL fibrils. Although no damage was incurred in the initial equilibrium step, the higher GAG molecule concentration, and consequently, the higher GAG swelling pressure in the MZ caused the MZ to fail at slightly lower ultimate tensile strain values compared to the SZ. In the MZ, higher GAG swelling pressure resulted in greater initial COL fibril strains following the initial equilibrium step. For the same value of E_N^D in the SZ and MZ, the greater initial COL strains in the MZ resulted in lower ultimate tensile strain values. The proposed CDAC model and the developed finite-element models were used to simulate AC damage, degradation, and ultimate tissue failure and to compare simulation results with experimental results. Thus, the hypothesis of this study was that a CDAC model utilizing independent anisotropic COL and isotropic GAG constitutive damage models could be used to model AC damage. The computational capability
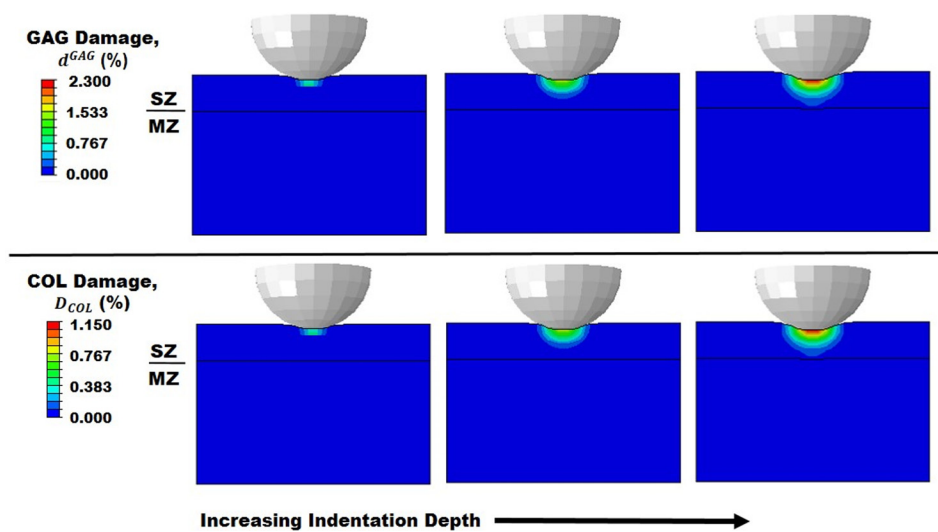
Fig. 10 Contour plots of (top) GAG damage parameter, d^{GAG}, and (bottom) COL fibril damage parameter, D_{col} with progressive spherical indentation loading in a bilayered AC model with discrete SZ (SZ and MZ). A rigid spherical indenter was displaced into the articular surface while displacements in all directions at the bottom of the MZ were held fixed. Damage parameters of $E_N^D = 0.15$, $d_{max}^{GAG} = 0.5$, and $\eta = 0.25$ were used. Mesh lines removed for clarity.

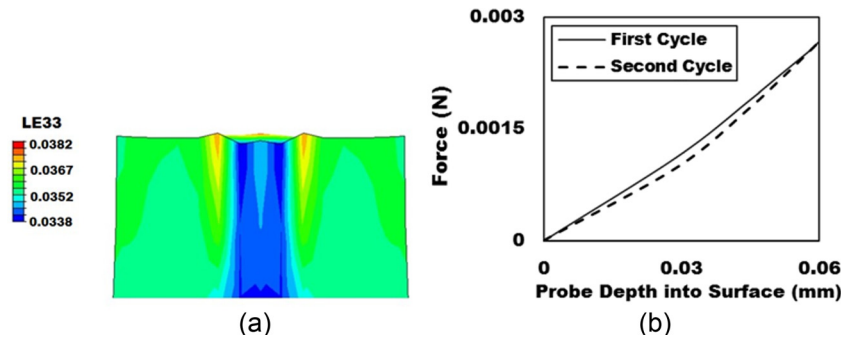**Fig. 11 Finite-element results. (*a*) A contour plot of LE strain perpendicular to the articular surface in the SZ showing cartilage thickening postdamage. Displacements are shown 100× for clarity. (*b*) Force versus displacement plots for two cycle indentation loading showing hysteresis and a decrease in reaction force in the second cycle compared to the first cycle.**

developed here will help researchers to better understand the mechanisms that lead to early stage OA and progress to late stage OA.

The spherical indentation finite-element simulation results from this work elucidate the potential damage response, and the constituent-specific consequences of overloading on AC. Some extent of validation of these indentation simulation results is possible through comparisons of the locations of COL and GAG damage between these modeling results and experimental studies. The experimental observation that GAG damage, which in this model is considered to be equivalent to reductions in GAG density, was found to occur predominantly in the superficial layers of AC with overloading [31] is in good agreement with the location of GAG damage calculated with our CDAC model. Another study observed that in OA, COL denaturation started at the articular surface [30] which is a result that is again in good agreement with our CDAC model results. Although this model predicts that damage initiates in the SZ, propagation of damage into the MZ is not presently simulated and may require additional development, such as element deletion and/or fatigue damage criteria. Additionally, through damage to the COL fibrils and the inherent osmotic swelling pressure of GAG molecules, the CDAC model predicts a postdamage increase in cartilage thickness that is consistent with previous observations of AC thickening with OA [22,49]. However, it is difficult to directly compare experimental results for AC thickening in OA with our model because the loading history of OA groups is unknown. These CDAC model results indicate that overloading that leads to AC damage may lead to AC thickening. In our CDAC model, swelling is indirectly modeled via a GAG molecule-induced osmotic pressure rather than an explicit swelling model as proposed by Lai et al. [50] or an intrafibrillar and extrafibrillar compartmental swelling model as proposed by Loret and Simões [51]. For the immature tissue studied here, the intrafibrillar and extrafibrillar compartmental model of AC is likely unnecessary due to the low GAG concentration [52]. In the future, work to include explicit AC swelling models may improve these CDAC model results. The spherical indentation simulation from this work introduces discrete SZ and MZ layers that are attached *via* tied contact constraints. Due to the inherent discrete nature of finite-element analysis, our model does not include a smooth transition between SZ and MZ regions. Therefore, the stiffer COL fibril modulus, and higher GAG molecule concentration in the MZ coupled with the strain-based damage theory presented here, effectively make the MZ much stiffer focusing deformations as well as damage in the softer SZ. The reduced load-carrying capacity with subsequent postdamage loading to the same indentation depth (Fig. 11) suggests that there is a reduced load-carrying capacity of AC following even small amounts of damage that may lead to further damage propagation under otherwise normal loading conditions. The spherical indentation simulations presented here provide insight into the specific constituent responses as well as the overall AC tissue response to loading which induces damage.

The CDAC model presented in this paper is subject to several limitations. For example, the CDAC model is currently calibrated only for newborn bovine AC from the patellofemoral groove because there was not a comprehensive data set in terms of age, depth, anatomical site, and species available for another tissue source. Also, the GAG constituent damage model implies that even for small volumetric compression that may be experienced during normal physiological loading GAG damage will occur. However, the GAG damage function, d^{GAG} is proposed such that small volumetric compressions will not result in significant GAG damage. Additionally, time-dependent effects, such as viscoelasticity and poroelasticity, have been neglected. Thus, this CDAC model represents the equilibrium response of AC, and all time-dependent effects, such as the viscoelasticity of COL fibrils and poroelasticity of the solid MAT of AC, are neglected. Therefore, a direct experimental validation of the tensile and/or compressive failure results presented in this work would require extremely slow experimental strain rates (i.e., strain rate approaching zero) not currently available in the literature. The CDAC model does represent a first step toward a complete time-dependent model of AC damage, and currently, the CDAC model could be used to simulate focal defects and other early injuries to AC both in vivo and in vitro. Due to the great number of experimental biomechanical and biochemical parameters required for a complete validation of this CDAC model, the present work is presented without complete validation. It should be noted that all of the constituent parameters implemented in this CDAC model including COL fibril and GAG damage parameters are likely subject to large inherent biological variations with respect to factors, such as species, anatomical location, age, disease state, and loading history.

Several constitutive assumptions regarding the mechanical behavior of COL fibrils were required for the implementation of the CDAC model. One such assumption is that the mechanical response of a single COL fibril is linearly elastic up to the failure strain. A previous study successfully modeled the experimental behavior of newborn bovine AC from the patellofemoral groove using a constant fibril modulus [32]. However, this assumption may not be appropriate for more mature AC tissue or for AC from a different source. Another assumption is the complete and immediate failure of COL fibrils strained beyond the Lagrangian failure strain parameter, E_N^D which is supported by an imaging study that observed COL fibril rupture and failure [53] likely leading to a complete loss of the mechanical integrity of damaged COL fibrils. A different postyield COL fibril behavior (e.g., COL fibril softening) and/or the inclusion of time-dependent effects may better capture the macroscopic AC damage response observed experimentally in uniaxial tension [3,54] and tensile fatigue [55–57].

This CDAC model of COL fibril damage is presented in a rigorous and general sense that allows for differential COL fibril failure behaviors to be implemented with additional experimental results. In this CDAC model, finite deformations of the macroscopic tissue lead to progressive COL fibril recruitment, and with sufficient deformations, subsequent COL damage that progresses through fibrils originally oriented in different directions. Due to the progressive loading behavior of the COL fibrils, the damage response of AC tissue is dependent on the initial COL fibril distribution and the direction of loading. The alteration of the effective distribution of COL fibrils in AC due to damage (Fig. 8) may have profound effects on the propagation of damage and the evolution of OA. With additional experimental observations, future studies may improve the accuracy of the assumptions made here regarding COL fibril behavior.

The mechanical damage response of AC in our CDAC model has been shown to be highly dependent on the COL fibril Lagrangian failure strain in direction N, E_N^D. However, precise values of E_N^D have not yet been established. Molecular computational modeling studies have suggested that COL fibrils are capable of attaining large deformations between 15% and 45%, which is the range of the COL fibril failure strains studied in this work [58,59]. An additional molecular modeling study examined the failure behavior of COL fibrils showing that structural fibril parameters, such as fibril length, fibril diameter, and crosslink density, had an effect on fibril failure properties in uniaxial stress in tension [59]. An experimental study using self-assembled uncrosslinked type I COL fibers found fiber failure strains between 24% and 68% strain [60]. To the best of our knowledge, there exists no concise description of the failure behavior or the failure strain of type II COL fibrils. Experimental studies coupled with a fitting of this model to experimental failure data may provide a method of determining an exact value for the COL fibril Lagrangian failure strain, E_N^D.

The GAG constituent damage model presented here hypothesizes that the maximum volumetric contraction in the loading history of AC results in an effective decrease in GAG molecule density as a result of GAG molecule leeching (i.e., GAG molecules pushed out of the tissue) and/or cleaving (i.e., GAG molecules breaking rendering them ineffective). Note that here there are no conclusions drawn with regard to the precise mechanism(s) of GAG damage. Thus, a potential limitation of the proposed GAG damage formulation is that only maximum volumetric decrease rather than cyclical loading results in GAG damage. Additionally, interactions between COL fibrils and GAG molecules may affect GAG damage evolution wherein damaged fibrils are no longer able to retain GAG molecules in the solid MAT of AC. Although there is no exact validation of the proposed GAG damage model, several studies suggest that GAG damage may occur in AC during loading and in OA. To the best of our knowledge, there is no consensus regarding the precise mechanisms that cause GAG damage. Thus, this model of GAG damage is presented as an example to propose one way that decreases in GAG concentration as observed experimentally may occur. For example, single impact overloading has been experimentally shown to lead to damage in AC [61,62] indicating that one-time overload scenarios can damage GAG molecules. An experimental study [63] showed in mature bovine cartilage that both cell death and GAG loss, which in this work is considered to be equivalent to GAG damage, occurred starting from the articular surface following short-term cyclical injury level loading (∼6 hrs). Another study found GAG molecule and COL fibril fragments in tissue media following loading [64] suggesting that loading can cause GAG molecules to disassociate from the tissue solid MAT. With chemical depletion of GAG molecules, experimental studies have shown a diminished compressive response of AC tissue compared with normal AC [65,66]. Furthermore with severe OA, alterations in GAG concentration have been observed compared with healthy AC tissue [17,67] as well as alterations in GAG molecule structure and synthesis [68]. Although the precise mechanism of GAG damage remains unknown, the GAG damage model proposed in this work establishes an example method for modeling a decrease in effective GAG concentration and consequently a decrease in GAG osmotic pressure as observed experimentally during loading and OA scenarios. Future experimental work to develop an understanding of the precise mechanisms of GAG molecule damage can be directly incorporated into this model by implementing alternative functions for d^{GAG}.

Our CDAC model has demonstrated a capability to model constituent-specific damage and tensile failure in AC that likely lead to OA in vivo. Spherical indentation results demonstrate the experimentally observed locations of AC tissue damage in early term OA as well as cartilage overloading. Although limited simulation results are presented, the goal of this work is to introduce the CDAC model and to outline constitutive development and implementation thereof. Future studies may use this model to study differential loading conditions and to expand the model to include fatigue damage behavior and/or element deletion criteria to more clearly demonstrate progressive damage behavior. Mesh convergence studies for the uniaxial tension and spherical indentation simulations indicated that both models had sufficiently refined meshes. However, as with other damage models, the CDAC model demonstrated mesh-dependent localization of damage. Further work to expand the CDAC model to include nonlocal effects or enhanced gradient damage methods could be implemented to eliminate mesh-dependent damage localization [69,70]. Further experimental work may enable more precise validation of this model including the exact functional form of GAG molecule damage and a type II COL fibril postyield behavior and Lagrangian failure strain value. Additional computational work is proposed to expand this model to include development of constituent-based viscoelastic and poroelastic properties to implement a time-dependent capability of this model and enable more realistic in vivo damage simulations and comparisons with experimental data. Future experimental and computational studies that improve the precision of these results could be used to help treat OA patients and at-risk individuals. For example, one potential extension of this model would be to identify exercises or movements that may serve to mitigate the progression of AC damage for patients that are at already at a high risk for OA. These results may help to elucidate the mechanisms and consequences of damage and degradation, which lead to OA as well as traumatic AC injuries.

Acknowledgment

Appendix

COL Fibril Damage Parameter Evolution. The COL fibril damage parameter is specifically proposed as

$$d_N^f = H(\gamma_N^f) \tag{A1}$$

where γ_N^f is a dimensionless COL fibril damage-related ISV in direction N. For this study, all COL fibrils are assumed to be initially undamaged and thus, all initial values of $\gamma_{N_{(0)}}^f = 0$ are set such that $d_{N_{(0)}}^f = 0$. With the intention of presenting a complete general theory, additional assumptions are required and introduced to define the evolution and history of COL fibril damage. All COL fibril damage history parameters are evaluated in each discrete direction N at each material point. First, the COL damage function, f_N^{COL}, which tracks COL fibril damage in each direction N at a material point is introduced as

$$f_N^{\text{COL}} = -H(E_N - E_N^D) \qquad (A2)$$

where H is the Heaviside step function operator, E_N is the current COL fibril directional Lagrangian strain, and E_N^D is the Lagrangian failure strain of a COL fibril (i.e., the maximum elastic strain of a COL fibril). If $E_N > E_N^D$ then $f_N^{\text{COL}} = -1$ and additional COL fibril damage has occurred in direction N. If $E_N \leq E_N^D$ then $f_N^{\text{COL}} = 0$ and no additional COL fibril damage has been incurred. An additional relationship is defined as

$$\delta\gamma_N^{\text{f}} - f_N^{\text{COL}} \qquad (A3)$$

where $\delta\gamma_N^{\text{f}}$ is the incremental change of the COL damage ISV, γ_N^{f}. For the case of $f_N^{\text{COL}} = 0$, Eq. (A3) gives $\delta\gamma_N^{\text{f}} = 0$ meaning that additional damage has not occurred and there is no evolution of the damage-like ISV, γ_N^{f}. For $f_N^{\text{COL}} = -1$, Eq. (A3) gives $\delta\gamma_N^{\text{f}} = 1$. Note that because $\delta\gamma_N^{\text{f}} \geq 0$ healing and/or repair of COL fibrils is effectively disallowed as the value of γ_N^{f} can never decrease. An example of the stress–strain response for a fibril in direction N with E_N^D is shown below in Fig. 1. In essence, for all $\delta\gamma_N^{\text{f}} \geq 1$ from Eq. (A1), $d_N^{\text{f}} = 1$, which represents a fully degraded fibril stress in the direction N. Note that this formulation is presented with the capability to easily implement alternative forms for d_N^{f}, and thus Eqs. (A1)–(A3) are presented independently.

COL Fibril Constituent Stress and Material Stiffness Tensors. Using Eq. (6) and applying the chain rule as shown below

$$\frac{\partial\psi^{\text{COL}}}{\partial\mathbf{C}} = \frac{\partial\psi^{\text{COL}}}{\partial E_N}\frac{\partial E_N}{\partial\mathbf{C}} \qquad (A4)$$

the following result for the COL constituent second Piola-Kirchhoff stress tensor, $\mathbf{S}^{\text{COL}}$ is derived:

$$\mathbf{S}^{\text{COL}} = \frac{1}{4}\int_{\phi=0}^{2\pi}\int_{\theta=0}^{\pi}\left[\delta(E_N)\frac{1}{2}\varphi_N^{\text{f}}E^{\text{f}2}E_N\left[1 - H(\gamma_N^{\text{f}})\right]\right.$$
$$\left. + H(E_N)\varphi_N^{\text{f}}E^{\text{f}}E_N\left[1 - H(\gamma_N^{\text{f}})\right]\right][\mathbf{N}\otimes\mathbf{N}]\sin\theta\,d\theta\,d\phi \quad (A5)$$

For the integral, the first term is zero because the Dirac-Delta function $\delta(E_N)$ evaluates the integrand at $E_N = 0$, which leads to multiplication by $E_N = 0$, resulting in a zero term. The second term is the nonzero term and is reported in Eq. (12). To derive the COL constituent material stiffness tensor Eq. (12) is used in Eq. (6) applying the chain rule as shown below in

$$\frac{\partial\mathbf{S}^{\text{COL}}}{\partial\mathbf{C}} = \frac{\partial\mathbf{S}^{\text{COL}}}{\partial E_N}\frac{\partial E_N}{\partial\mathbf{C}} \qquad (A6)$$

giving the following result via a straightforward derivation:

$$\mathbb{C}_{\text{ABCD}}^{\text{COL}} = \frac{1}{4\pi}\int_{\phi=0}^{2\pi}\int_{\theta=0}^{\pi}\left[\delta(E_N)\varphi_N^{\text{f}}E^{\text{f}}E_N[1 - H(\gamma_N^{\text{f}})]\right.$$
$$\left. + H(E_N)\varphi_N^{\text{f}}E^{\text{f}}[1 - H(\gamma_N^{\text{f}})]\right]N_A N_B N_C N_D\sin\theta\,d\theta\,d\phi$$
$$(A7)$$

The same cancelation of the first term in the integral of Eq. (A7) as used in the derivation of the COL second Piola-Kirchhoff stress gives the result reported in Eq. (13).

Clausius–Duhem Inequality. The Clausius–Duhem inequality ensures that the dissipation and damage-related terms introduced in this model are thermodynamically consistent at finite strain.

Note that the polyconvexity is satisfied as in Stender et al. [32] yet, the additional damage terms presented must also be thermodynamically correct. The Clausius–Duhem inequality for a single COL fibril in direction N assuming uniaxial stress, isothermal conditions, and homogeneous temperature can be written with respect to the reference configuration as

$$S_N^{\text{COL}}\dot{E}_N - \dot{\psi} \geq 0 \qquad (A8)$$

where S_N^{COL} and $\dot{E}_N$ are the uniaxial COL second Piola-Kirchhoff stress and Lagrangian strain rate in the direction N, respectively, and ψ is the Helmholtz free energy function per unit reference volume. The true COL fibril Helmholtz free energy function per unit reference volume, ψ^{f} is assumed to be a combination of elastic and damage terms as written below

$$\psi^{\text{f}}(E_N, E_N^D, \gamma_N^{\text{f}}) = H(E_N)\frac{1}{2}E^{\text{f}}(E_N)^2[1 - H(\gamma_N^{\text{f}})] \qquad (A9)$$

Taking the material time derivative of ψ^{f}, neglecting any density changes in a single fibril, and substituting into Eq. (A8) gives the following result:

$$\left(S_N^{\text{COL}} - \frac{\partial(\psi^{\text{f}})}{\partial E_N}\right)\dot{E}_N - \frac{\partial(\psi^{\text{f}})}{\partial\gamma_N^{\text{f}}}\dot{\gamma}_N^{\text{f}} \geq 0 \qquad (A10)$$

For clarity, the derivative terms are shown to be

$$\frac{\partial(\psi^{\text{f}})}{\partial E_N} = \delta(E_N)\frac{1}{2}E^{\text{f}}(E_N)^2[1 - H(\gamma_N^{\text{f}})] + H(E_N)E^{\text{f}}E_N[1 - H(\gamma_N^{\text{f}})]$$
$$(A11)$$

and

$$\frac{\partial(\psi^{\text{f}})}{\partial\gamma_N^{\text{f}}} = -H(E_N)\frac{1}{2}E^{\text{f}}(E_N)^2\delta(\gamma_N^{\text{f}}) \qquad (A12)$$

Note that the first term of Eq. (A11) leads to zero integral over the reference configuration because $\delta(E_N)$ when evaluated within an integral over various pyramidal angles returns the integrand at $E_N = 0$ which results in a zero multiplication. In order to satisfy Eq. (A10) for arbitrary $\dot{E}_N$, the following result is derived for the true COL fibril second Piola Kirchhoff stress in direction N as:

$$S_N^{\text{COL}} = H(E_N)E^{\text{f}}E_N[1 - H(\gamma_N^{\text{f}})] \qquad (A13)$$

Thus, combining Eqs. (A10) and (A12), the remaining inequality must hold

$$H(E_N)\frac{1}{2}E^{\text{f}}(E_N)^2\delta(\gamma_N^{\text{f}})\dot{\gamma}_N^{\text{f}} \geq 0 \qquad (A14)$$

which is satisfied for $E^f > 0$ noting that $\dot{\gamma}_N^f \geq 0$. In this work, the true COL fibril properties are expanded to the total COL properties by integrating spatially which gives the results presented in the text.

The Clausius–Duhem inequality for the GAG constituent is written with respect to the reference configuration as

$$\frac{1}{2}\mathbf{S}^{\text{GAG}}:\dot{\mathbf{C}} - \dot{\psi}^{\text{GAG}} \geq 0 \qquad (A15)$$

Taking the material time derivative of $\psi^{\text{GAG}}(J, \beta)$ gives the following result:

$$\dot{\psi}^{\text{GAG}} = (\partial(\psi^{\text{GAG}})/\partial\mathbf{C})\dot{\mathbf{C}} + (\partial(\psi^{\text{GAG}})/\partial\beta)\dot{\beta} \qquad (A16)$$

The chain rule is applied to the $\partial(\psi^{\text{GAG}})/\partial\mathbf{C}$ term in Eq. (A15) as follows:

$$\left(\partial(\psi^{\text{GAG}})/\partial\mathbf{C}\right) = \left(\partial(\psi^{\text{GAG}})/\partial J\right)(\partial J/\partial\mathbf{C}) \tag{A17}$$

Noting that $\partial J/\partial\mathbf{C} = (1/2)J\mathbf{C}^{-1}$ and substituting Eq. (A17) into Eq. (A16) gives the result shown below

$$\dot{\psi}^{\text{GAG}} = \left(\frac{1}{2}\frac{\partial(\psi^{\text{GAG}})}{\partial J}J\mathbf{C}^{-1}\right)\dot{\mathbf{C}} + \frac{\partial(\psi^{\text{GAG}})}{\partial\beta}\dot{\beta} \tag{A18}$$

Substituting Eq. (A18) into Eq. (A15) and rearranging terms give the following result:

$$\left(\frac{1}{2}\mathbf{S}^{\text{GAG}} - \frac{1}{2}\frac{\partial(\psi^{\text{GAG}})}{\partial J}J\mathbf{C}^{-1}\right):\dot{\mathbf{C}} - \frac{\partial(\psi^{\text{GAG}})}{\partial\beta}\dot{\beta} \geq 0 \tag{A19}$$

For clarity, the derivative terms are given below

$$\frac{\partial(\psi^{\text{GAG}})}{\partial J} = -\alpha_1\left(\frac{\rho_0^{\text{GAG}}}{J}\right)^{\alpha_2}\left\{1 - d_{\max}^{\text{GAG}}\left[e^{\left(\frac{-\beta}{\eta}\right)} - e^{\left(\frac{-1}{\eta}\right)}\right]\right\} \tag{A20}$$

and

$$\frac{\partial(\psi^{\text{GAG}})}{\partial\beta} = -\alpha_1\alpha_2\frac{(\rho_0^{\text{GAG}})^{\alpha_2}}{J^{(\alpha_2-1)}}\left\{\frac{d_{\max}^{\text{GAG}}}{\eta}\left[e^{\left(\frac{-\beta}{\eta}\right)}\right]\right\} \tag{A21}$$

In order to satisfy Eq. (A19) for any arbitrary $\dot{\mathbf{C}}$, the following result is given for the GAG second Piola-Kirchhoff stress tensor, $\mathbf{S}^{\text{GAG}}$:

$$\mathbf{S}^{\text{GAG}} = J\mathbf{F}^{-1}\left(-\alpha_1\left(\frac{\rho_0^{\text{GAG}}}{J}\right)^{\alpha_2}\left\{1 - d_{\max}^{\text{GAG}}\left[e^{\left(\frac{-\beta}{\eta}\right)} - e^{\left(\frac{-1}{\eta}\right)}\right]\right\}\right)\mathbf{F}^{-\text{T}} \tag{A22}$$

Additionally, to fully satisfy Eq. (A19), the following inequality must also hold:

$$\alpha_2\frac{(\rho_0^{\text{GAG}})^{\alpha_2}J^{(1-\alpha_2)}}{(1-\alpha_2)}\left\{\frac{d_{\max}^{\text{GAG}}}{\eta}\left[e^{\left(\frac{-\beta}{\eta}\right)}\right]\right\}\dot{\beta} \geq 0 \tag{A23}$$

Equation (A23) is satisfied, when $\alpha_1 \geq 0$, $\rho_0^{\text{GAG}} \geq 0$, $\alpha_2 > 1$, $d_{\max}^{\text{GAG}} \geq 0$, $\eta \geq 0$, and $\dot{\beta} \leq 0$ as presented herein. Note that Eq. (19) ensures that $\delta\beta \leq 0$, and thus, $\dot{\beta} \leq 0$.

References

[1] Maroudas, A., Bayliss, M. T., and Venn, M. F., 1980, "Further Studies on the Composition of Human Femoral Head Cartilage," Ann. Rheum. Dis., **39**(5), pp. 514–523.

[2] Brocklehurst, R., Bayliss, M. T., Maroudas, A., Coysh, H. L., Freeman, M. A. R., Revell, P. A., and Ali, S. Y., 1984, "The Composition of Normal and Osteoarthritic Articular Cartilage From Human Knee Joints," J. Bone Jt. Surg. Am., **66**(1), pp. 95–106.

[3] Asanbaeva, A., Tam, J., Schumacher, B. L., Klisch, S. M., Masuda, K., and Sah, R. L., 2008, "Articular Cartilage Tensile Integrity: Modulation by Matrix Depletion is Maturation-Dependent," Arch. Biochem. Biophys., **474**(1), pp. 175–182.

[4] Kiviranta, P., Rieppo, J., Korhonen, R. K., Julkunen, P., Töyräs, J., and Jurvelin, J. S., 2006, "Collagen Network Primarily Controls Poisson's Ratio of Bovine Articular Cartilage in Compression," J. Orthop. Res., **24**(4), pp. 690–699.

[5] Ficklin, T., Thomas, G., Barthel, J. C., Asanbaeva, A., Thonar, E. J., Masuda, K., Chen, A. C., Sah, R. L., Davol, A., and Klisch, S. M., 2007, "Articular Cartilage Mechanical and Biochemical Property Relations Before and After In Vitro Growth," J. Biomech., **40**(16), pp. 3607–3614.

[6] Williams, G. M., Dills, K. J., Flores, C. R., Stender, M. E., Stewart, K. M., Nelson, L. M., Albert, C. C., Masuda, K., Hazelwood, S. J., Klisch, S. M., and Sah, R. L., 2010, "Differential Regulation of Immature Articular Cartilage Compressive Moduli and Poisson's Ratios by In Vitro Stimulation With IGF-1 and TGF-β1," J. Biomech., **43**(13), pp. 2501–2507.

[7] Maroudas, A., and Bannon, C., 1981, "Measurement of Swelling Pressure in Cartilage and Comparison With the Osmotic Pressure of Constituent Proteoglycans," Biorheology, **18**(3–6), pp. 619–632.

[8] Asanbaeva, A., Masuda, K., Thonar, E. J.-M. A., Klisch, S. M., and Sah, R. L., 2007, "Mechanisms of Cartilage Growth: Modulation of Balance Between Proteoglycan and Collagen In Vitro Using Chondroitinase ABC," Arthritis Rheum., **56**(1), pp. 188–198.

[9] Maroudas, A., 1976, "Balance Between Swelling Pressure and Collagen Tension in Normal and Degenerate Cartilage," Nature, **260**(5554), pp. 808–809.

[10] Thomas, G. C., Asanbaeva, A., Vena, P., Sah, R. L., and Klisch, S. M., 2009, "A Nonlinear Constituent Based Viscoelastic Model for Articular Cartilage and Analysis of Tissue Remodeling Due to Altered Glycosaminoglycan-Collagen Interactions," ASME J. Biomech. Eng., **131**(10), p. 101002.

[11] Kuettner, K. E., 1992, "Biochemistry of Articular Cartilage in Health and Disease," Clin. Biochem., **25**(3), pp. 155–163.

[12] Williamson, A. K., Chen, A. C., and Sah, R. L., 2001, "Compressive Properties and Function—Composition Relationships of Developing Bovine Articular Cartilage," J. Orthop. Res., **19**(6), pp. 1113–1121.

[13] Buckwalter, J. A., and Mankin, H. J., 1998, "Articular Cartilage Repair and Transplantation," Arthritis Rheum., **41**(8), pp. 1331–1342.

[14] Noyes, F. R., and Stabler, C. L., 1989, "A System for Grading Articular Cartilage Lesions at Arthroscopy," Am. J. Sports Med., **17**(4), pp. 505–513.

[15] Curl, W. W., Krome, J., Gordon, E. S., Rushing, J., Smith, B. P., and Poehling, G. G., 1997, "Cartilage Injuries: A Review of 31,516 Knee Arthroscopies," Arthroscopy: J. Arthroscopy Relat. Surg., **13**(4), pp. 456–460.

[16] Botter, S. M., van Osch, G. J. V. M., Waarsing, J. H., van der Linden, J. C., Verhaar, J. A. N., Pols, H. A. P., van Leeuwen, J. P., and Weinans, H., 2008, "Cartilage Damage Pattern in Relation to Subchondral Plate Thickness in a Collagenase-Induced Model of Osteoarthritis," Osteoarthritis Cartilage, **16**(4), pp. 506–514.

[17] Temple-Wong, M. M., Bae, W. C., Chen, M. Q., Bugbee, W. D., Amiel, D., Coutts, R. D., Lotz, M., and Sah, R. L., 2009, "Biomechanical, Structural, and Biochemical Indices of Degenerative and Osteoarthritic Deterioration of Adult Human Articular Cartilage of the Femoral Condyle," Osteoarthritis Cartilage, **17**(11), pp. 1469–1476.

[18] Wong, B. L., Kim, S. H. C., Antonacci, J. M., McIlwraith, C. W., and Sah, R. L., 2010, "Cartilage Shear Dynamics During Tibio-Femoral Articulation: Effect of Acute Joint Injury and Tribosupplementation on Synovial Fluid Lubrication," Osteoarthritis Cartilage, **18**(3), pp. 464–471.

[19] Novakofski, K. D., Williams, R. M., Fortier, L. A., Mohammed, H. O., Zipfel, W. R., and Bonassar, L. J., 2014, "Identification of Cartilage Injury Using Quantitative Multiphoton Microscopy," Osteoarthritis Cartilage, **22**(2), pp. 355–362.

[20] Maroudas, A., and Venn, M., 1977, "Chemical Composition and Swelling of Normal and Osteoarthrotic Femoral Head Cartilage. II. Swelling," Ann. Rheum. Dis., **36**(5), pp. 399–406.

[21] Saarakkala, S., Julkunen, P., Kiviranta, P., Mäkitalo, J., Jurvelin, J. S., and Korhonen, R. K., 2010, "Depth-Wise Progression of Osteoarthritis in Human Articular Cartilage: Investigation of Composition, Structure and Biomechanics," Osteoarthritis Cartilage, **18**(1), pp. 73–81.

[22] Cotofana, S., Buck, R., Wirth, W., Roemer, F., Duryea, J., Nevitt, M., Eckstein, F., and Osteoarthritis Initiative Investigators Group, 2012, "Cartilage Thickening in Early Radiographic Knee Osteoarthritis: A Within-Person, Between-Knee Comparison," Arthritis Care Res., **64**(11), pp. 1681–1690.

[23] Rodríguez, J. F., Cacho, F., Bea, J. A., and Doblaré, M., 2006, "A Stochastic-Structurally Based Three Dimensional Finite-Strain Damage Model for Fibrous Soft Tissue," J. Mech. Phys. Solids, **54**(4), pp. 864–886.

[24] Calvo, B., Peña, E., Martinez, M. A., and Doblaré, M., 2007, "An Uncoupled Directional Damage Model for Fibred Biological Soft Tissues. Formulation and Computational Aspects," Int. J. Numer. Methods Eng., **69**(10), pp. 2036–2057.

[25] Rodriguez, J. F., Alastrue, V., and Doblare, M., 2008, "Finite Element Implementation of a Stochastic Three Dimensional Finite-Strain Damage Model for Fibrous Soft Tissue," Comput. Methods Appl. Mech. Eng., **197**(9), pp. 946–958.

[26] Gajewski, T., Weisbecker, H., Holzapfel, G. A., and Lodygowski, T., 2013, "Implementation of a Hyperelastic Model for Arterial Layers Considering Damage and Distributed Collagen Fiber Orientations."

[27] Weisbecker, H., Pierce, D. M., Regitnig, P., and Holzapfel, G. A., 2012, "Layer-Specific Damage Experiments and Modeling of Human Thoracic and Abdominal Aortas With Non-Atherosclerotic Intimal Thickening," J. Mech. Behav. Biomed. Mater., **12**, pp. 93–106.

[28] Famaey, N., Vander Sloten, J., and Kuhl, E., 2013, "A Three-Constituent Damage Model for Arterial Clamping in Computer-Assisted Surgery," Biomech. Model. Mechanobiol., **12**(1), pp. 123–136.

[29] Hosseini, S. M., Wilson, W., Ito, K., and van Donkelaar, C. C., 2014, "A Numerical Model to Study Mechanically Induced Initiation and Progression of Damage in Articular Cartilage," Osteoarthritis Cartilage, **22**(1), pp. 95–103.

[30] Hollander, A. P., Pidoux, I., Reiner, A., Rorabeck, C., Bourne, R., and Poole, A. R., 1995, "Damage to Type II Collagen in Aging and Osteoarthritis Starts at the Articular Surface, Originates Around Chondrocytes, and Extends Into the Cartilage With Progressive Degeneration," J. Clin. Invest., **96**(6), pp. 2859–2869.

[31] Rolauffs, B., Muehleman, C., Li, J., Kurz, B., Kuettner, K. E., Frank, E., and Grodzinsky, A. J., 2010, "Vulnerability of the Superficial Zone of Immature Articular Cartilage to Compressive Injury," Arthritis Rheum., **62**(10), pp. 3016–3027.

[32] Stender, M. E., Raub, C. B., Yamauchi, K. A., Shirazi, R., Vena, P., Sah, R. L., Hazelwood, S. J., and Klisch, S. M., 2012, "Integrating qPLM and Biomechanical Test Data With an Anisotropic Fiber Distribution Model and Predictions of TGF-β1 and IGF-1 Regulation of Articular Cartilage Fiber Modulus," Biomech. Model. Mechanobiol., 12(6), pp. 1073–1088.

[33] Schröder, J., and Neff, P., 2003, "Invariant Formulation of Hyperelastic Transverse Isotropy Based on Polyconvex Free Energy Functions," Int. J. Solids Struct., 40(2), pp. 401–445.

[34] Davison, L., Stevens, A. L., and Kipp, M. E., 1977, "Theory of Spall Damage Accumulation in Ductile Metals," J. Mech. Phys. Solids, 25(1), pp. 11–28.

[35] Lanir, Y., 1983, "Constitutive Equations for Fibrous Connective Tissues," J. Biomech., 16(1), pp. 1–12.

[36] Lei, F., and Szeri, A. Z., 2006, "The Influence of Fibril Organization on the Mechanical Behaviour of Articular Cartilage," Proc. R. Soc. A, 462(2075), pp. 3301–3322.

[37] Ateshian, G. A., 2007, "Anisotropy of Fibrous Tissues in Relation to the Distribution of Tensed and Buckled Fibers," ASME J. Biomech. Eng., 129(2), pp. 240–249.

[38] Ateshian, G. A., Rajan, V., Chahine, N. O., Canal, C. E., and Hung, C. T., 2009, "Modeling the Many Observed Phenomena," ASME J. Biomech. Eng., 131(6), p. 061003.

[39] Shirazi, R., Vena, P., Sah, R. L., and Klisch, S. M., 2011, "Modeling the Collagen Fibril Network of Biological Tissues as a Nonlinearly Elastic Material Using a Continuous Volume Fraction Distribution Function," Math. Mech. Solids, 16(7), pp. 706–715.

[40] Williamson, A. K., Chen, A. C., Masuda, K., Thonar, E. J.-M. A., and Sah, R. L., 2003, "Tensile Mechanical Properties of Bovine Articular Cartilage: Variations With Growth and Relationships to Collagen Network Components," J. Orthop. Res., 21(5), pp. 872–880.

[41] Buschmann, M., and Grodzinsky, A., 1995, "A Molecular Model of Proteoglycan-Associated Forces in Cartilage Mechanics," ASME J. Biomech. Eng., 117(2), pp. 179–192.

[42] McCormack, T., and Mansour, J. M., 1997, "Reduction in Tensile Strength of Cartilage Precedes Surface Damage Under Repeated Compressive Loading in vitro," J. Biomech., 31(1), pp. 55–61.

[43] Bae, W. C., Temple, M. M., Amiel, D., Coutts, R. D., Niederauer, G. G., and Sah, R. L., 2003, "Indentation Testing of Human Cartilage: Sensitivity to Articular Surface Degeneration," Arthritis Rheum., 48(12), pp. 3382–3394.

[44] Temple, M. M., Bae, W. C., Chen, M. Q., Lotz, M., Amiel, D., Coutts, R. D., and Sah, R. L., 2007, "Age- and Site-Associated Biomechanical Weakening of Human Articular Cartilage of the Femoral Condyle," Osteoarthritis Cartilage, 15(9), pp. 1042–1052.

[45] Wilson, W., van Donkelaar, C. C., van Rietbergen, B., and Huiskes, R., 2005, "A Fibril-Reinforced Poroviscoelastic Swelling Model for Articular Cartilage," J. Biomech., 38(6), pp. 1195–1204.

[46] Wilson, W., Huyghe, J. M., and Donkelaar, C. C., 2006, "Depth-Dependent Compressive Equilibrium Properties of Articular Cartilage Explained by Its Composition," Biomech. Model. Mechanobiol., 6(1–2), pp. 43–53.

[47] Davol, A., Bingham, M. S., Sah, R. L., and Klisch, S. M., 2007, "A Nonlinear Finite Element Model of Cartilage Growth," Biomech. Model. Mechanobiol., 7(4), pp. 295–307.

[48] Wilson, W., van Donkelaar, C. C., van Rietbergen, R., and Huiskes, R., 2005, "The Role of Computational Models in the Search for the Mechanical Behavior and Damage Mechanisms of Articular Cartilage," Med. Eng. Phys., 27(10), pp. 810–826.

[49] Buck, R. J., Wyman, B. T., Le Graverand, M. P., Hudelmaier, M., Wirth, W., Eckstein, F., and A9001140 Investigators, 2009, "Does the Use of Ordered Values of Subregional Change in Cartilage Thickness Improve the Detection of Disease Progression in Longitudinal Studies of Osteoarthritis?," Arthritis Rheum., 61(7), pp. 917–924.

[50] Lai, W. M., Hou, J. S., and Mow, V. C., 1991, "A Triphasic Theory for the Swelling and Deformation Behaviors of Articular Cartilage," ASME J. Biomech. Eng., 113(3), pp. 245–258.

[51] Loret, B., and Simões, F. M., 2004, "Articular Cartilage With Intra-and Extrafibrillar Waters: A Chemo-Mechanical Model," Mech. Mater., 36(5), pp. 515–541.

[52] Oungoulian, S., 2007, "Articular Cartilage Constitutive Modeling: A Polyconvex Strain Energy Function for Proteoglycan and Validation of a Growth Mixture Model With Collagen Remodeling: A Thesis," Master's dissertation, California Polytechnic State University, San Luis Obispo, CA.

[53] Sasazaki, Y., Shore, R., and Seedhom, B. B., 2006, "Deformation and Failure of Cartilage in the Tensile Mode," J. Anat., 208(6), pp. 681–694.

[54] Asanbaeva, A., Masuda, K., Thonar, E. J.-M. A., Klisch, S. M., and Sah, R. L., 2007, "Regulation of Immature Cartilage Growth by IGF-I, TGF-β1, BMP-7, and PDGF-AB: Role of Metabolic Balance Between Fixed Charge and Collagen Network," Biomech. Model. Mechanobiol., 7(4), pp. 263–276.

[55] Weightman, B., 1976, "Tensile Fatigue of Human Articular Cartilage," J. Biomech., 9(4), pp. 193–200.

[56] Weightman, B., Chappell, D. J., and Jenkins, E. A., 1978, "A Second Study of Tensile Fatigue Properties of Human Articular Cartilage," Annals of the Rheumatic Diseases, 37(1), pp. 58–63.

[57] Bellucci, G., and Seedhom, B. B., 2002, "Tensile Fatigue Behaviour of Articular Cartilage," Biorheology, 39(1), pp. 193–199.

[58] Buehler, M. J., 2007, "Molecular Nanomechanics of Nascent Bone: Fibrillar Toughening by Mineralization," Nanotechnology, 18(29), p. 295102.

[59] Tang, Y., Ballarini, R., Buehler, M. J., and Eppell, S. J., 2010, "Deformation Micromechanisms of Collagen Fibrils Under Uniaxial Tension," J. R. Soc. Interface, 7(46), pp. 839–850.

[60] Pins, G. D., and Silver, F. H., 1995, "A Self-Assembled Collagen Scaffold Suitable for Use in Soft and Hard Tissue Replacement," Mater. Sci. Eng.: C, 3(2), pp. 101–107.

[61] Jeffrey, J. E., Thomson, L. A., and Aspden, R. M., 1997, "Matrix Loss and Synthesis Following a Single Impact Load on Articular Cartilage In Vitro," Biochim. Biophys. Acta, 1334(2), pp. 223–232.

[62] Bush, P., Hodkinson, P., Hamilton, G., and Hall, A., 2005, "Viability and Volume of Bovine Articular Chondrocytes? Changes Following a Single Impact and Effects of Medium Osmolarity," Osteoarthritis Cartilage, 13(1), pp. 54–65.

[63] Lin, P., 2004, "Increased Stromelysin-1 (MMP-3), Proteoglycan Degradation (3B3- and 7D4) and Collagen Damage in Cyclically Load-Injured Articular Cartilage," Osteoarthritis Cartilage, 12(6), pp. 485–496.

[64] Thibault, M., Robin Poole, A., and Buschmann, M. D., 2002, "Cyclic Compression of Cartilage/Bone Explants In Vitro Leads to Physical Weakening, Mechanical Breakdown of Collagen and Release of Matrix Fragments," J. Orthop. Res., 20(6), pp. 1265–1273.

[65] Korhonen, R. K., Laasanen, M. S., Töyräs, J., Lappalainen, R., Helminen, H. J., and Jurvelin, J. S., 2003, "Fibril Reinforced Poroelastic Model Predicts Specifically Mechanical Behavior of Normal, Proteoglycan Depleted and Collagen Degraded Articular Cartilage," J. Biomech., 36(9), pp. 1373–1379.

[66] Rieppo, J., Töyräs, J., Nieminen, M. T., Kovanen, V., Hyttinen, M. M., Korhonen, R. K., Jurvelin, J. S., and Helminen, H. J., 2003, "Structure-Function Relationships in Enzymatically Modified Articular Cartilage," Cells Tissues Organs, 175(3), pp. 121–132.

[67] Appleyard, R., 2003, "Topographical Analysis of the Structural, Biochemical and Dynamic Biomechanical Properties of Cartilage in an Ovine Model of Osteoarthritis," Osteoarthritis Cartilage, 11(1), pp. 65–77.

[68] Rizkalla, G., Reiner, A., Bogoch, E., and Poole, A. R., 1992, "Studies of the Articular Cartilage Proteoglycan Aggrecan in Health and Osteoarthritis. Evidence for Molecular Heterogeneity and Extensive Molecular Changes in Disease," J. Clin. Invest., 90(6), pp. 2268–2277.

[69] Peerlings, R. H. J., Geers, M. G. D., De Borst, R., and Brekelmans, W. A. M., 2001, "A Critical Comparison of Nonlocal and Gradient-Enhanced Softening Continua," Int. J. Solids Struct., 38(44), pp. 7723–7746.

[70] Buehler, M. J., and Ackbarow, T., 2008, "Nanomechanical Strength Mechanisms of Hierarchical Biological Materials and Tissues," Comput. Methods Biomech. Biomed. Eng., 11(6), pp. 595–607.